

# Residual-based attention and connection to information bottleneck theory in PINNs

Sokratis J. Anagnostopoulos<sup>a,1</sup>, Juan Diego Toscano<sup>b,1</sup>,  
Nikolaos Stergiopoulos<sup>a</sup>, George Em Karniadakis<sup>b,c</sup>

<sup>a</sup>*Laboratory of Hemodynamics and Cardiovascular Technology,  
EPFL, Lausanne, 1015, VD, Switzerland*

<sup>b</sup>*School of Engineering, Brown University, Providence, 02912, RI, USA*

<sup>c</sup>*Division of Applied Mathematics, Brown University, Providence, 02912, RI, USA*

---

## Abstract

Driven by the need for more efficient and seamless integration of physical models and data, physics-informed neural networks (PINNs) have seen a surge of interest in recent years. However, ensuring the reliability of their convergence and accuracy remains a challenge. In this work, we propose an efficient, gradient-less weighting scheme for PINNs, that accelerates the convergence of dynamic or static systems. This simple yet effective attention mechanism is a function of the evolving cumulative residuals and aims to make the optimizer aware of problematic regions at no extra computational cost or adversarial learning. We illustrate that this general method consistently achieves a relative  $L^2$  error of the order of  $10^{-5}$  using standard optimizers on typical benchmark cases of the literature. Furthermore, by investigating the evolution of weights during training, we identify two distinct learning phases reminiscent of the fitting and diffusion phases proposed by the information bottleneck (IB) theory. Subsequent gradient analysis supports this hypothesis by aligning the transition from high to low signal-to-noise ratio (SNR) with the transition from fitting to diffusion regimes of the adopted weights. This novel correlation between PINNs and IB theory could open future possibilities for understanding the underlying mechanisms behind the training and stability of PINNs and, more broadly, of neural operators.

*Keywords:* Residual-based attention, PINNs convergence accuracy, information bottleneck theory, self-adaptive weights.

---

<sup>1</sup>The first two authors contributed equally to this work

## 1. Introduction

Physics-informed neural networks (PINNs) offer an alternative to traditional numerical methods for solving partial differential equations (PDEs) in forward and inverse problems[1]. In the PINN approach, a neural network is trained to approximate the solution of a PDE by minimizing a composite loss function that includes terms related to the physical laws and data from initial boundary conditions, simulations, or experiments [2]. Keeping a balance between the loss terms is crucial to avoid convergence and accuracy issues, especially when dealing with highly nonlinear, multi-scale, or chaotic behavior problems[3, 4, 5]. To address this imbalance, researchers have developed several approaches that can be roughly classified into three categories: neural network modifications, PDE transformations, and adaptive weighting strategies.

A neural network modification addresses the multi-layer perceptron optimization capabilities via model reparametrizations [6, 7], input dimension expansions [8, 9], sequential learning [10, 11], or adaptive activation functions [12]. On the other hand, PDE transformations attempt to simplify the problem by enforcing the physical laws in their homologous forms. For instance, by implementing the PDE on its constrained expression, the number of losses can be reduced, and the optimizer can focus on a single condition [13, 14, 15]. Similarly, by using alternate or auxiliary physical laws, it is possible to reduce the number of equations or decrease the PDE order [16, 17], which eases the optimization process.

Adaptive weighting strategies address the loss imbalances by iteratively altering the contribution of particular terms or regions of the domain during the training process. This modification can be done indirectly by adaptively resampling points in crucial areas [18, 19, 20] or directly by assigning multipliers that adjust the contribution of each error function. For instance, Wang et al.,[6] proposed a learning rate annealing algorithm that balances the losses' weights based on their back-propagated gradients. Wang et al. [3] also defined a causal parameter for time-dependent problems that force the model to learn sequentially based on the time steps. Global multipliers generally modify the average contribution of each loss term [6, 3, 21, 22]. Similarly, these multipliers can be applied locally (i.e., per training point); McCLENNY et al. [4] proposed a self-adaptive (SA) method where the loss weights are trained via adversarial training. Zhang et al. [23] extended this concept and proposed a differentiable adversarial self-adaptive (DASA) pointwise weighting

scheme that uses a subnetwork to find the optimal weights. These weighting strategies enhance the capabilities of PINNs and enable them to address challenging problems in diverse fields. Nevertheless, their implementation can be expensive since they require coupling auxiliary networks [23], training additional multipliers [4], or computing and processing gradients [6]. Moreover, some of these approaches grow unboundedly [4, 17] and do not relate to the neural network training capabilities, which may result in over-refining some regions while ignoring others, as pointed out by [23].

To address these problems, we propose a bounded residual-based attention (RBA) scheme that efficiently computes adaptive weights for the collocation points based on the residuals of the given PDEs. The suggested weighting approach considers the neural network training dynamics and adapts itself during the training process. Furthermore, as the optimizer significantly exceeds the accuracy threshold of the vanilla PINN, we observe two distinct learning phases, evident in the evolution of weight distributions. We perform subsequent gradient analysis, and we associate this behavior with the information bottleneck (IB) theory, which proposes an optimal method to devise a condensed representation of an input while preserving the majority of information related to an output [24, 25]. This approach employs the concept of mutual information, which measures the knowledge gained about one random variable through the observation of another. According to the IB theory, a well-functioning model should retain essential output information while discarding insignificant input details, thereby creating an “information bottleneck” [26, 27, 28].

This paper is organized as follows. In Section 2, we provide an overview of PINNs, introduce the RBA weighting scheme, and review additional modifications that enhance the model performance. Then, in Section 3, we present the implementation of our method through two benchmark problems and conduct an ablation study to interpret the relative contribution of each modification. In Section 4, we analyze the evolution of our multipliers during training and link their behavior with the bottleneck theory. Finally, in Section 5, we summarize the findings and discuss our future work. In the appendix, we include details regarding the implementation.

## 2. Methods

### 2.1. Physics-Informed Neural networks

In the context of Physics-Informed Neural Networks (PINNs), a general partial differential equation (PDE) can be expressed as:

$$\mathcal{L}\{u(x, t)\} = f(x, t), \quad (1)$$

where  $u(x, t)$  is the unknown function we wish to approximate,  $\mathcal{L}$  denotes the differential operator, and  $f(x, t)$  is a given source or forcing function that introduces external influences to the system. The differential operator  $\mathcal{L}$  depends on the specific PDE under consideration. For instance, in the case of the heat equation,  $\mathcal{L} = \frac{\partial}{\partial t} - \kappa \nabla^2$ , where  $\kappa$  is the thermal diffusivity and  $\nabla^2$  is the Laplace operator.

Additionally, the problem may be constrained by several types of boundary conditions. These conditions are typically categorized into Dirichlet, Neumann, Robin, or Periodic, and are represented as follows:

$$u(x_b, t) = g_d(x_b, t), \quad (\text{Dirichlet}) \quad (2)$$

$$\frac{\partial u}{\partial n}(x_b, t) = g_n(x_b, t), \quad (\text{Neumann}) \quad (3)$$

$$\alpha u(x_b, t) + \beta \frac{\partial u}{\partial n}(x_b, t) = g_r(x_b, t), \quad (\text{Robin}) \quad (4)$$

$$u(x + L, t) = u(x, t), \quad (\text{Periodic}) \quad (5)$$

where  $x_b$  denotes the boundary points. The Dirichlet condition defines the function value at the boundary, the Neumann condition specifies the normal derivative at the boundary, and the Robin condition is a weighted combination of the function and its normal derivative. For the Periodic condition, the function value repeats after a certain length  $L$ .

The loss function in PINNs is designed to encompass the deviation of the neural network solution from the initial conditions, boundary conditions, and the PDE itself. The influence of these components in the loss function is balanced using Lagrange multipliers  $\lambda_r$ ,  $\lambda_{ic}$  and  $\lambda_{bc}$ :

$$\mathcal{L} = \lambda_{ic} \cdot \mathcal{L}_{ic} + \lambda_{bc} \cdot \mathcal{L}_{bc} + \lambda_r \cdot \mathcal{L}_r, \quad (6)$$

where  $\mathcal{L}_{ic}$ ,  $\mathcal{L}_{bc}$ , and  $\mathcal{L}_r$  represent the losses associated with the initial conditions, boundary conditions, and the residuals of the PDE, respectively. In general, each loss term  $\mathcal{L}_i$  takes the form:

$$\mathcal{L}_i = \langle h_i(u_{NN}) \rangle, \quad \text{for } i \in \{ic, bc, r\} \quad (7)$$

where  $\langle \cdot \rangle$  is the mean operator and  $h_i$  is a function of the neural network  $u_{NN}$ , associated with the error between the prediction and the ground truth.

Each of these terms encourages the neural network to conform to the respective physical laws or initial/boundary conditions encoded in the problem. The Lagrange multipliers can be global (e.g., scalars balancing each individual loss term) or local (e.g., vectors balancing each collocation or boundary point). In the most basic PINN definition,  $\lambda = 1$  for all loss terms.

The training of the neural network weights is performed using an optimization method like stochastic gradient descent (SGD). In each iteration  $k$ , an update is applied to a weight  $w$  as follows:

$$w^{k+1} = w^k - \eta \cdot \nabla_w \mathcal{L}, \quad (8)$$

where  $\eta$  is the learning rate, and  $\nabla_w \mathcal{L}$  is the gradient of the loss function with respect to  $w$ . This process iteratively reduces the loss, pushing the solution towards satisfying the given PDE and boundary/initial conditions.

## 2.2. Residual-based attention (RBA) scheme

One of the inherent challenges in obtaining accurate results with PINNs is that the residuals of key collocation points can get overlooked by the mean calculation of the objective function (Eq. 7). Consequently, despite a decrease in total loss during training, certain spatial or temporal characteristics might not be fully captured. This issue becomes particularly pronounced in multiscale problems, where such troublesome areas could not only result in a lack of detail but could also impair the flow of important information from the initial and boundary conditions into the domain of interest, thereby hindering convergence. Although mini-batching techniques present a potential solution to this issue, the difficult task of a priori identifying the problematic regions remains.

A workaround for this problem is selecting a set of Lagrange multipliers, either global or local, which can be adjustable during training. The aim of the global multipliers is to balance different terms of the loss function, while local multipliers aim at weighting the influence of specific collocation points of the

domain. Establishing a systematic rule for updating these multipliers can significantly aid the optimizer, with several successful strategies documented in the literature, demonstrating major improvements to the vanilla PINNs performance [3, 4, 23].

Furthermore, as opposed to classical numerical methods, which can guarantee stability, the training convergence of PINNs is affected by the evolution of residuals which will have some degree of stochasticity, leading to a corresponding degree of instability. Driven by the aforementioned challenges, the initial objective of this work is the development of a simple, gradient-less weighting scheme based on the rolling history of the cumulative residuals to extend the attention span of the optimizer. The proposed scheme aims to increase attention to the challenging regions of information propagation in both space and time dimensions defining the problem.

The update rule for the proposed residual-based Lagrange multipliers for any collocation point  $i$  on iteration  $k$  is given by:

$$\lambda_i^{k+1} \leftarrow \gamma \lambda_i^k + \eta^* \frac{|r_i|}{\max_i(|r_i|)}, \quad i \in \{0, 1, \dots, N_r\}, \quad (9)$$

where  $N_r$  is the number of collocation points,  $r_i$  is the PDE residual for point  $i$ ,  $\gamma$  is the decay parameter and  $\eta^*$  is the learning rate, respectively. Note that the learning rate of the optimizer  $\eta$  and the learning rate of the weighting scheme  $\eta^*$  are two different hyperparameters.

This is a convergent linear homogeneous recurrence relation. Given that  $\frac{|r_i|}{\max_i(|r_i|)} \in [0, 1]$  and  $\lambda_i^0 \neq 0, \forall i \in \{0, 1, \dots, N_r\}$ , its bounds are given by:

$$\lambda_i^k \in \left(0, \frac{\eta^*}{1 - \gamma}\right], \quad \text{as } k \rightarrow \infty. \quad (10)$$

These local multipliers scale with the normalized cumulative residuals, but they also behave dynamically during training due to the decay  $\gamma$  as follows: since  $\gamma$  lies between 0 and 1,  $\lambda^k$  will gradually decrease in its contribution to  $\lambda^{k+1}$ , as  $k$  increases. Simultaneously,  $\eta^* \frac{|r_i|}{\max(|r_j|)}$  is being added in each iteration, leading to an eventual equilibrium. However, as different points  $i$  may be targeted depending on the stage of the training process, the distribution of  $\lambda_i$  will dynamically vary across the domain of interest.

The main advantages of the proposed residual weighting scheme are summarized as follows:

1. Deterministic operation scheme, bounded by the  $\gamma$  and  $\eta^*$  parameters, which ensure the absence of exploding multipliers.

2. No training or gradient calculation is involved, leading to negligible additional computational cost.
3. Scaling with the cumulative residuals guarantees increased attention on the solution fronts where the PDEs are unsatisfied in both spatial and temporal dimensions.

The modified training process for an indicative standard Gradient Descent optimization method is outlined in Algorithm 1. We define the RBA weights as  $\lambda_i$  and initialize them with 0 values for all collocation points, noting that  $\lambda_i = \sqrt{\lambda_r}$  (from Eq. 6). For all training examples, the RBA learning rate and decay hyperparameters are set as  $\eta^* = 0.01$  and  $\gamma = 0.999$ , respectively. A constant  $c$  may be added to the updated weights to raise the lower bound and adjust the ratio  $\max(\lambda_i)/\min(\lambda_i)$  (for this study  $c = 0$ ).

---

**Algorithm 1:** Residual-based attention Gradient Descent

---

**Data:** Training set, learning rates  $\eta, \eta^*$ , decay  $\gamma$ , lower bound  $c$

**Result:** Optimized parameters  $w_i, i \in \{0, 1, \dots, N_r\}$

Initialization: Xavier [29]  $\forall w_i$  and  $0 \forall \lambda_i$ ;

**while** *stopping condition not met* **do**

**for** *each batch of examples in the training set* **do**

$$\lambda_i^{k+1} \leftarrow \gamma \lambda_i^k + \eta^* \frac{|r_i|}{\max_i(|r_i|)};$$

$$\lambda_i^{k+1} \leftarrow \lambda_i^{k+1} + c;$$

$$\mathcal{L}_r^* = \langle (\lambda_i \cdot r_i)^2 \rangle;$$

$$\mathcal{L} = \lambda_{ic} \mathcal{L}_{ic} + \lambda_{bc} \mathcal{L}_{bc} + \mathcal{L}_r^*;$$

$$w_i^{k+1} = w_i^k - \eta \cdot \nabla_w \mathcal{L};$$

**end**

**end**

---

### 2.3. Additional PINN enhancements

#### 2.3.1. Modified multi-layer perceptrons

For the design of the network architecture, we leverage the recently introduced modified multi-layer perceptron (mMLP) [6], which draws its inspiration from the attention mechanisms prominent in transformers [30]. The mMLP aims at augmenting the efficacy of PINNs by embedding the input variables  $x$  into the hidden states of the network. Initially, these inputs are encoded in a feature space by employing two distinct encoders,  $U$  and  $V$ .

They are then assimilated within each hidden layer of a conventional MLP by point-wise multiplication. The encoders are given by:

$$U = \sigma(x^0 w^U + b^U), \quad V = \sigma(x^0 w^V + b^V) \quad (11)$$

We implement a variation of this concept by performing the encoding operation right before each activation function, as it performed better for our experiments. Thus, each forward pass is defined as:

$$\alpha^l(x) = \alpha^{l-1}(x)w^l + b^l, \quad \text{for } l \in \{1, 2, \dots, \text{layers}\} \quad (12)$$

$$\alpha^l(x) = (1 - \alpha^l(x)) \odot U + \alpha^l(x) \odot V \quad (13)$$

$$\alpha^l(x) = \sigma(\alpha^l(x)) \quad (14)$$

where  $x$  is the input,  $\alpha^l$  and  $w^l$  are the neurons and weights of layer  $l$ ,  $\sigma$  is the activation function and  $\odot$  is the element-wise product.

### 2.3.2. Exact imposition of boundary conditions

The inexact imposition of boundary conditions can negatively affect the accuracy and training stability of neural networks [31, 6, 32].

*Dirichlet Boundary Conditions.* A recent study by Sukumar et al. [13] showed how to impose Dirichlet, Neuman, and Robin boundary conditions in PINNs by using approximate distance functions (ADF). The constrained expression for Dirichlet boundary conditions is defined in equation 15.

$$u(\mathbf{x}) = g(\mathbf{x}) + \phi(\mathbf{x})u_{NN}(\mathbf{x}), \quad (15)$$

where  $g(\mathbf{x})$  is a function that satisfies  $u$  along the boundaries,  $u_{NN}(\mathbf{x})$  is the output of our neural network, and  $\phi(\mathbf{x})$  is a composite distance function that equals zero when evaluated on the boundaries. If the boundary is composed of  $M$  partitions  $[S_1, \dots, S_M]$ , the composite distance function for Dirichlet boundary conditions can be described as:

$$\phi(\phi_1, \phi_2, \dots, \phi_M) = \prod_i^M \phi_i, \quad (16)$$

where  $[\phi_1, \dots, \phi_M]$  are the individual distance functions. Notice that if  $\mathbf{x} \in S_i$ , then  $\phi(\mathbf{x}) = 0$  and the neural network approximation exactly satisfies the boundary conditions, i.e.,  $u(\mathbf{x}) = g(\mathbf{x})$ .



*Periodic Boundary Conditions.* Similarly, it is possible to enforce periodic boundary conditions as hard constraints strictly by constructing Fourier feature embeddings of the input data [3, 31]. In particular, the periodic constraint of a smooth function  $u(x)$  can be encoded in a neural network using a one-dimensional Fourier feature embedding (See equation 17).

$$v(x, y) = [1, \cos(\omega_x x), \sin(\omega_x x), \dots, \cos(m\omega_x x), \sin(m\omega_x x)] \quad (17)$$

In the same way, a neural network can incorporate 2D periodic constraints by utilizing a two-dimensional Fourier feature embedding [3].

$$p(x, y) = \begin{bmatrix} \cos(\omega_x x)\cos(\omega_y y), \dots, \cos(n\omega_x x)\cos(m\omega_y y) \\ \cos(\omega_x x)\sin(\omega_y y), \dots, \cos(n\omega_x x)\sin(m\omega_y y) \\ \sin(\omega_x x)\cos(\omega_y y), \dots, \sin(n\omega_x x)\cos(m\omega_y y) \\ \sin(\omega_x x)\sin(\omega_y y), \dots, \sin(n\omega_x x)\sin(m\omega_y y) \end{bmatrix} \quad (18)$$

where,  $w_x = \frac{2\pi}{P_x}$ ,  $w_y = \frac{2\pi}{P_y}$ ,  $m, n$  are a non-negative integers, and  $P_x$  and  $P_y$  are the periods in the  $x$  and  $y$  directions. Dong et al. [31] proved that any network representation  $u_{NN}(v(x))$  and  $u_{NN}(p(x, y))$  are periodic in the  $x$  and  $y$  directions, respectively.

### 3. Results

#### 3.1. Dynamic case: 1D Allen-Cahn equation

The Allen-Cahn equation is a compelling benchmark for PINNs due to its challenging characteristics. It is regarded as a “stiff” PDE, a term that describes equations that require careful numerical handling to avoid instability in their solutions. This complexity arises from its ability to produce solutions with pronounced, sharp transitions in both spatial and temporal dimensions. The 1D Allen-Cahn PDE is given by:

$$\frac{\partial u}{\partial t} = 10^{-4} \frac{\partial^2 u}{\partial x^2} - 5u^3 + 5u, \quad (19)$$

with initial condition and periodic boundary conditions:

$$u(0, x) = x^2 \cos(\pi x), \quad \forall x \in [-1, 1], \quad (20)$$

$$u(t, x + 1) = u(t, x - 1), \quad \forall t \geq 0 \quad \text{and} \quad x \in [-1, 1]. \quad (21)$$

To obtain the solution of Allen-Cahn PDE in Figure 1, we train a PINN for  $3 \cdot 10^5$  iterations with the standard Adam optimizer [33] and an exponential learning rate scheduler on 25600 collocation points. For the periodic boundary conditions, we use the formulation of section 2.3.2 and set  $\lambda_{ic} = 100$ , following the benchmark setup of the recent literature [3]. The rest of the parameters are mentioned in the appendix. The benchmark comparison of the final relative  $L^2$  error obtained by different methods is presented in Table 1, where the error for the RBA weights represents the average of five runs with random seeds. It should be noted that only the best performing methods of Table 1 ([3], [23]) utilize the PINN enhancements discussed in section 2.3. The relative  $L^2$  is defined as:

$$\text{relative } L^2 = \frac{\|Exact - Predicted\|_2}{\|Exact\|_2} \quad (22)$$

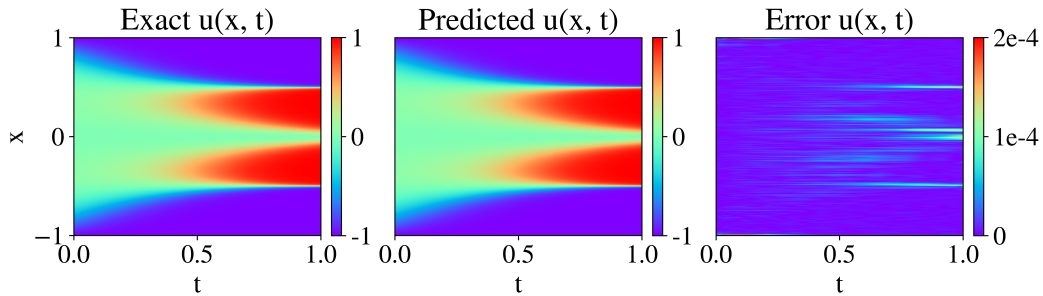


Figure 1: Exact solution of the 1D Allen-Cahn with the corresponding network prediction and the absolute error difference.

Method	Relative $L^2$ error
Vanilla PINN [1]	4.98e - 1
Self-adaptive weights [4]	2.1e - 2
Time marching [34]	1.68e - 2
Causal training [3]	1.39e - 4
DASA-PINNs [23]	8.57e - 5
<b>RBA weights</b>	<b>5.7e - 5</b>

Table 1: Relative  $L^2$  comparison between different methods of the literature for the 1D Allen-Cahn equation. The RBA run represents the average of five randomly chosen seeds.

### 3.1.1. Ablation Study for Allen-Cahn

An ablation study involves measuring the performance of a system after removing one or more of its components to measure the relative contribution of the ablated components [35]. To investigate the effect of the adopted methods on the relative  $L^2$  convergence, we perform a single-component ablation study and report the results in Table 2. The best-performing model of Table 1 is selected to represent the full model. For each run, a component is removed to identify the effect of the omitted method on the performance. Figure 2 shows the convergence histories of each run. As evident from these results, the coupling of the RBA scheme along with the Fourier feature embedding is the most important component to achieving low relative  $L^2$ . Moreover, the RBA weights initiate a steep convergence trajectory at 12000 iterations, achieving a final  $L^2$  of  $3.16 \cdot 10^{-3}$  without any additional component. Combined with the modified MLP and the Fourier features, the full model leads to the best  $L^2$  at  $4.5 \cdot 10^{-5}$ . The adopted mMLP accelerates the convergence in the first 60000 iterations, while it does not provide significant accuracy gains in the long run. The noise associated with the best-performing methods indicates that the optimizer is “jumping” over local minima of the loss landscape and effectively not getting stuck in a bad solution.

Method	Relative $L^2$ error
RBA	3.16 - 3
RBA+mMLP	3.79e - 3
mMLP+Fourier	3.2e - 4
RBA+Fourier	5.19e - 5
RBA+mMLP+Fourier	4.55e - 5

Table 2: Final relative  $L^2$  error for each case of the single-component ablation study on the 1D Allen-Cahn.

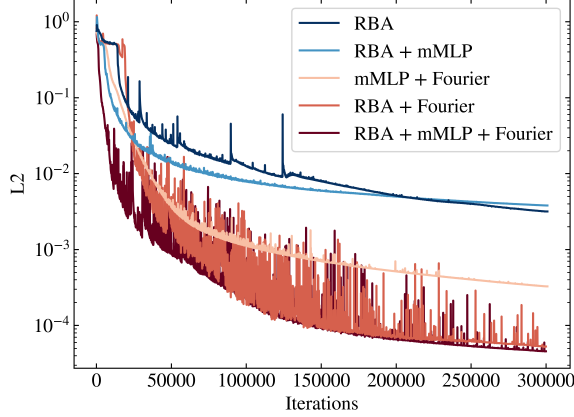


Figure 2: **Ablation study convergence for the 1D Allen-Cahn:** Progression of convergence for each experiment. The results clearly demonstrate that the integration of the RBA approach and the Fourier feature embedding is crucial for attaining a minimal relative  $L^2$ . When combined with a modified MLP architecture, an optimal  $L^2$  of  $4.5 \cdot 10^{-5}$  is reached. The implemented mMLP aids in speeding up the convergence during the initial 60000 iterations. Additionally, the RBA weights address the instability issues in the standard PINN, achieving a relative  $L^2$  of  $3.16 \cdot 10^{-3}$  without supplementary components. The noise linked with the top-performing methods suggests that the optimization process successfully avoids becoming trapped in sub-optimal solutions by effectively “leaping” past local minima in the loss landscape.

### 3.2. Static case: 2D Helmholtz equation

The Helmholtz equation is commonly employed to model wave and diffusion phenomena, capturing changes over time in either a spatial or combined spatial-temporal domain. The 2D Helmholtz PDE is expressed as follows:

$$\frac{\partial^2 u}{\partial x^2} + \frac{\partial^2 u}{\partial y^2} + k^2 u - q(x, y) = 0 \quad (23)$$

$$\begin{aligned} q(x, y) = & - (a_1 \pi)^2 \sin(a_1 \pi x) \sin(a_2 \pi y) \\ & - (a_2 \pi)^2 \sin(a_1 \pi x) \sin(a_2 \pi y) \\ & + k \sin(a_1 \pi x) \sin(a_2 \pi y), \end{aligned} \quad (24)$$

where  $q(x, y)$  is the forcing term which leads to the analytical solution  $u(x, y) = \sin(a_1 \pi x) \sin(a_2 \pi y)$  [4]. The boundary conditions are defined as follows:

$$u(-1, y) = u(1, y) = u(x, -1) = u(x, 1) = 0 \quad (25)$$

To allow a direct comparison with previous studies, we set  $a_1 = 1$ ,  $a_2 = 4$ ,  $k = 1$  and follow the experimental setup described in [23], setting  $\lambda_{bc} = 100$ . We initially apply a combination of Dirichlet and Periodic boundary conditions, with the latter enforced using the Fourier feature embedding. However, to avoid encoding the PDE analytical solution (i.e.,  $\sin(\pi x) \sin(4\pi y)$ ), we expand our inputs (i.e.,  $x, y$ ) using a truncated embedding with  $m = n = 5$  (Eq. 26):

$$p(x, y) = \begin{bmatrix} \cos(\omega_x x) \cos(\omega_y y), \dots, \cos(n\omega_x x) \cos(n\omega_y y) \\ \cos(\omega_x x) \sin(\omega_y y), \dots, \cos(n\omega_x x) \sin(n\omega_y y) \\ \sin(\omega_x x) \cos(\omega_y y), \dots, \sin(n\omega_x x) \cos(n\omega_y y) \end{bmatrix} \quad (26)$$

Then, we approximate the solution of the PDE as  $u_F = u_{NN}(p(x, y))$ , where  $u_{NN}$  is the modified MLP. Additionally, to demonstrate the flexibility of RBA weights, we examine an additional case applying only Dirichlet boundaries with approximate distance functions (ADF). Towards this end, we split the BCs into four partitions, i.e.,  $y = 1$ ,  $y = -1$ ,  $x = 1$ , and  $x = -1$ , and use  $\phi = (x^2 - 1)(y^2 - 1)$  as the composite distance function. Based on equation 25 we define  $g(\mathbf{x}) = 0$  and approximate the solution of the Helmholtz equation as,

$$u_{ADF} = (x^2 - 1)(y^2 - 1)u_{NN}(x, y), \quad (27)$$

which exactly satisfies the BCs. We train our models (i.e.,  $u_F$  and  $u_{ADF}$ ) using the Adam optimizer for  $2 \cdot 10^4$  iterations, followed by L-BFGS for  $3 \cdot 10^3$  iterations, noting that the RBA weights can be deployed for both optimizers. Figure 3 illustrates the exact solution of the 1x4 Helmholtz PDE alongside the corresponding prediction obtained from the PINN. Furthermore, in Table 3, we compare the average  $L^2$  errors for the Fourier and ADF exact boundary imposition methods with the current state-of-the-art methods.

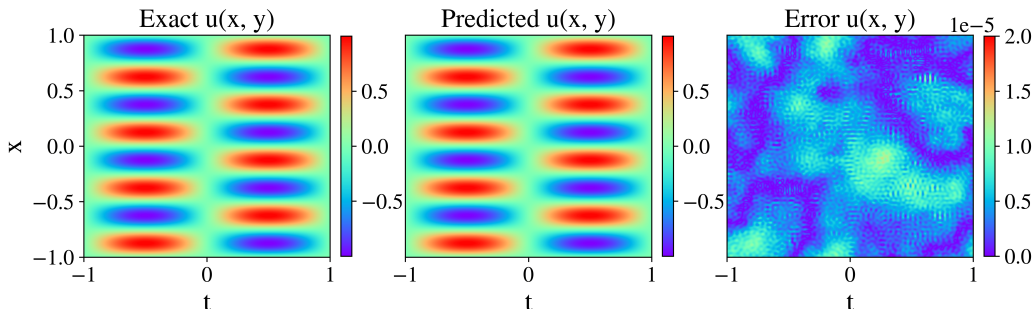


Figure 3: Analytical solution for the 2D Helmholtz equation and the corresponding network prediction with the absolute error difference.

Method	Relative $L^2$ error
Vanilla PINN [6]	8.14e - 2
Self-adaptive weights [4]	3.20e - 3
Learning-rate annealing [6]	1.49e - 3
DASA-PINNs [23]	5.35e - 5
RBA weights (ADF)	8.04e - 5
<b>RBA weights (Fourier)</b>	<b>1.46e - 5</b>

Table 3: Relative  $L^2$  comparison between different methods of the literature for the 2D Helmholtz equation. The RBA run represents the average of five randomly chosen seeds.

### 3.2.1. Ablation Study for Helmholtz

In this ablation study for the 2D Helmholtz, we present the convergence histories for each ablated system (Fig. 2) and summarize the final  $L^2$  errors in Table 4 and 5. For the first case (i.e.,  $u_F$ ), the Fourier feature embedding has the most significant influence in reaching a minimized relative  $L^2$ . The accuracy further improves paired with either the RBA scheme or the mMLP. The best-performing seed leads to an  $L^2$  of  $8.91 \cdot 10^{-6}$ ; however, we note that this method is employed for comparison purposes since the Fourier features incorporate the trigonometric traits of the analytical solution. Therefore, we also perform the same study using distance functions ( $u_{ADF}$ ), which indicates that the essential component is the ADF (Table 5). By exactly imposing boundary conditions, the number of loss terms is reduced, allowing the optimizer to focus on minimizing a single error function.

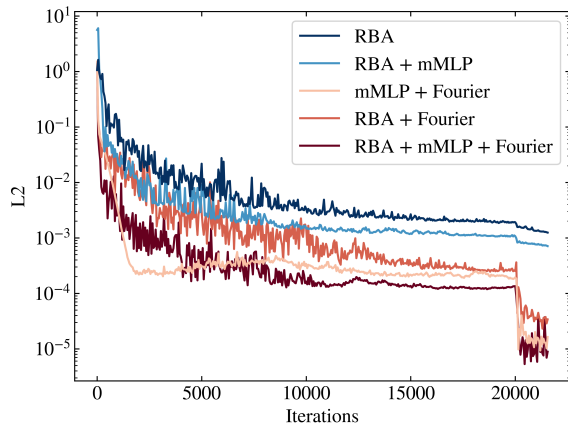


Figure 4: **Ablation study convergence for the 2D Helmholtz:** The convergence trajectory for each experiment is illustrated here. For this case, the Fourier feature embedding is critical in achieving a low relative  $L^2$ . Coupled with the RBA weights and a modified MLP architecture, the model reaches an optimal  $L^2$  of  $8.91 \cdot 10^{-6}$  after  $2 \cdot 10^4$  Adam and  $3 \cdot 10^4$  L-BFGS training steps.

Method	Relative $L^2$ error
RBA	1.25e - 3
RBA+mMLP	7.10e - 4
mMLP+Fourier	1.63e - 5
RBA+Fourier	3.04e - 5
RBA+mMLP+Fourier	8.91e - 6

Table 4: Final relative  $L^2$  error for each case of the ablation study on the 2D Helmholtz. The exact symmetry boundary condition is enforced using the Fourier feature embedding.

Method	Relative $L^2$ error
RBA	1.33e - 3
RBA+mMLP	7.40e - 4
mMLP+ADF	6.60e - 5
RBA+ADF	3.36e - 4
RBA+mMLP+ADF	5.33e - 5

Table 5: Final relative  $L^2$  error for 2D Helmholtz where the exact Dirichlet boundary condition is enforced using ADF.

### 3.3. RBA weight evolution

Figure 5 shows the evolution of RBA weights for the previously analyzed cases. For each run, the maximum value is bounded by Eq. 10, while the

upper bound for this study equals 10. The distribution of weights significantly varies depending on the stage of training; hence the maximum values fluctuate while approaching the upper bound. The fluctuation of the mean values is less pronounced until they finally converge to  $\approx 20\%$  of the upper bound. This behavior indicates that, on average, the total magnitude of weights remains constant while their distribution varies as the optimizer focuses on different parts of the domain. Thus, by introducing the decay factor  $\gamma$ , we can effectively prevent exploding weight values. At the same time, this allows the weights to be flexibly distributed, adapting as needed throughout different stages of the solution process.

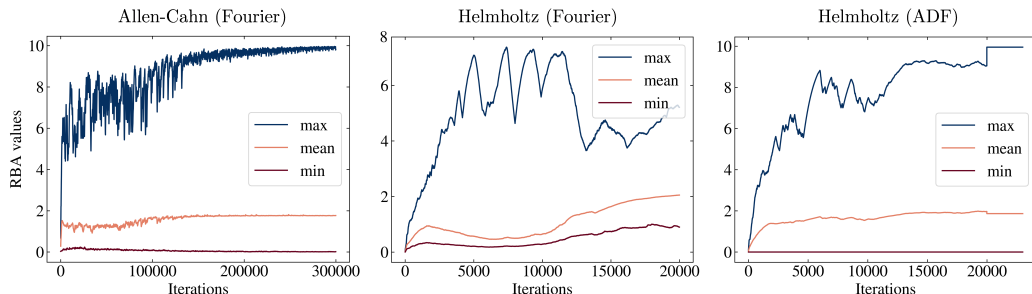


Figure 5: **Evolution of RBA weights.** For each case, the peak value is limited as per Eq. 10, with this study’s upper bound equaling 10. Notice that for the Helmholtz (Fourier) case, the RBA weights were only updated during Adam, indicating that the model did not fully converge. However, for the ADF the weights are updated during L-BFGS which pushes the maximum value to the upper bound after 20000 iterations. In general, the maxima fluctuate until they approach the upper limit during the final learning stages. On the other hand, the mean values show a less noticeable fluctuation before eventually stabilizing at about  $\approx 20\%$  of the upper bound. This trend indicates that, on average, the total magnitude of weights remains constant while their distribution adjusts dynamically as the optimizer shifts its focus across different domain sections.

#### 4. Information bottleneck (IB) theory

The information bottleneck theory was developed as a framework for understanding the trade-off between compression and prediction in supervised learning [24, 25]. It formulates an idealized principle for creating a compressed, or “bottlenecked,” representation of an input variable that retains as much information as possible about an output variable. The theory utilizes the concept of mutual information, which measures the amount of information obtained about one random variable by observing another. It proposes that a good model will retain all the relevant information about the output



while discarding irrelevant details about the input, creating an “information bottleneck.”

#### 4.1. *Fitting and Diffusion Phases of Learning*

Recently, it has been proposed that the process of deep learning can be divided into two primary phases: the fitting phase and the diffusion phase [26, 28].

1. **Fitting Phase:** In this phase, the model learns to correctly classify the training data, gradually reducing the empirical error. The model can memorize the data, building complex representations that fit the prediction set. This phase tends to decrease both the training and test errors and is characterized by a high Signal-to-Noise Ratio (SNR), indicating that the model is capturing more of the useful signal (important features of the data) compared to the noise (irrelevant or less meaningful details). In this context, “noise” is the random or unwanted information that does not contribute to the learning task.
2. **Diffusion Phase:** After the model has learned to fit the data, it continues to learn, but in a subtly different way. The network weights start to diffuse to improve the model’s generalization capabilities. The model simplifies the internal representations of the learned patterns by keeping the important features and discarding the irrelevant ones, thus effectively reducing the complexity of the representations. The training error remains the same in this phase, but the test error can decrease. The SNR also decreases as the model becomes more focused on preserving the meaningful signals and is less influenced by the noise. These two distinct phases can be seen as a process where the model first fits the data (captures relevant information) and then compresses it (discards irrelevant information), further enhancing its generalization ability.

#### 4.2. *Connection of IB theory to PINNs*

The benchmark examples demonstrate that the proposed residual-based method can extend the training accuracy beyond the original PINN formulation. Upon inspection of the weight evolution during the training process, we observed a behavior that largely met our expectations; the weights indeed form an ordered pattern consistent with the flow of information, primarily dictated by the initial conditions (Figs. 6,7). Yet, a surprising element

emerged as we noted an abrupt shift to chaotic patterns, occurring once the model descended below a specific test loss threshold (defined by the relative  $L^2$  error). Hence, two definite phases, akin to the “fitting” and “diffusion” from the IB theory, became apparent.

Following the formulation proposed by the IB theory, we performed a gradient analysis to quantify the transitions from high to low SNR. The normalized signal,  $\|\mu\|$  and noise,  $\|\sigma\|$  of the stochastic gradient distributions for each hidden layer  $l$  are given by:

$$\|\mu_l\| = \frac{\|\langle \nabla_w \mathcal{L}_i \rangle\|_F}{\|w_i\|_F} \quad (28)$$

$$\|\sigma_l\| = \frac{\|std(\nabla_w \mathcal{L}_i)\|_F}{\|w_i\|_F} \quad (29)$$

$$SNR = \frac{\|\mu_l\|}{\|\sigma_l\|}, \quad (30)$$

where  $i$  is the mini-batch and  $\|\cdot\|_F$  is the Forbenius norm. To apply this formulation, we divide our collocation points into 100 mini-batches and perform gradient calculations per batch for every 50 iterations of the optimizer without performing a backward pass. Hence, we deduce the batch-wise gradient information while the models are trained with the full batch.

We present the findings for the indicative 1D Allen-Cahn (Fig. 6) and 2D Helmholtz with  $a_1 = a_2 = 6$  (Fig. 7) runs. We define the three regimes of RBA weights evolution as Phase I (fitting), Phase II (transitional), and Phase III (diffusion). During these phases, the RBA weights undergo a swift change from order to disorder which is accompanied by a high to low  $SNR$  transition of the layer gradients, respectively. We also plot the normalized Loss and normalized relative  $L^2$  history to compare their convergence rates. In both cases, the convergence history of the normalized Loss and  $L^2$  indicates that the model continues to learn after the Loss has reached a plateau by further decreasing the  $L^2$  error. In addition, the magnitudes of the network’s weights  $\|w\|$  begin their final convergence trajectory at the beginning of the diffusive phase. For both examples, a fully connected MLP is used as it produces more pronounced transitions. It is important to mention that the convergence histories show the monotonic decrease of the Loss and  $L^2$  errors. The animations of the presented cases, along with the relevant code, will be available on <https://github.com/soanagno/rba-pinns>.

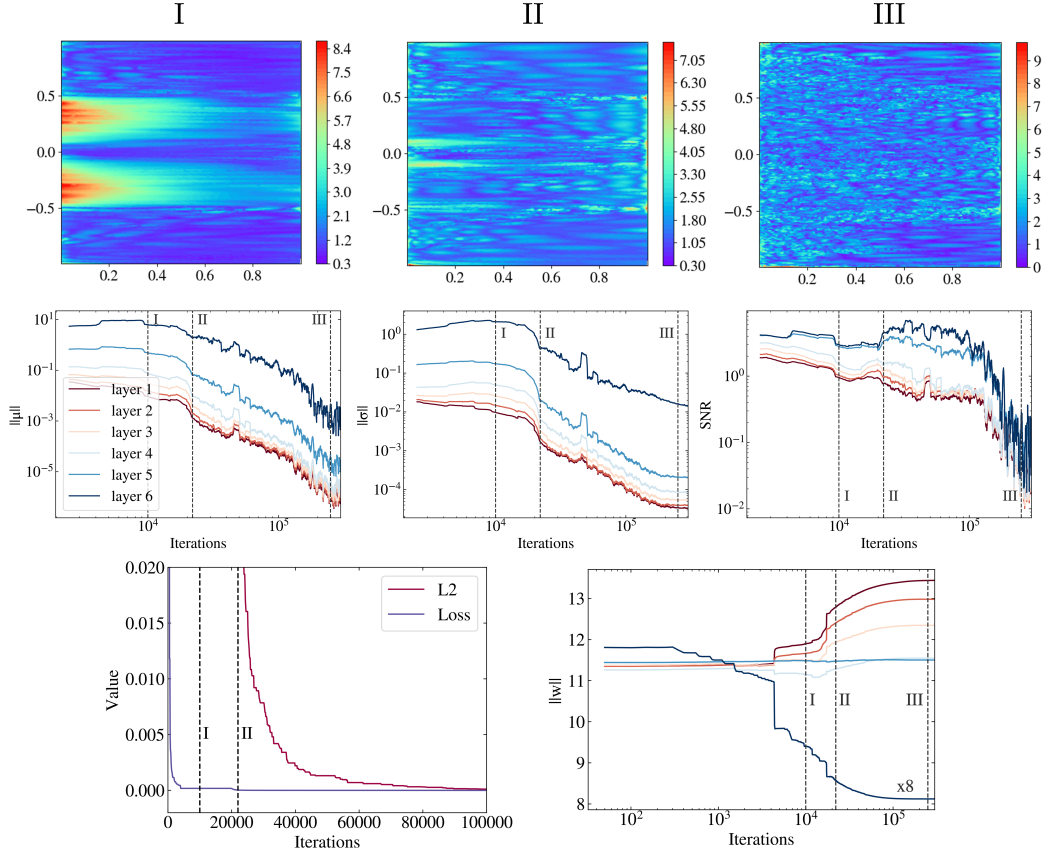


Figure 6: **Three phases of learning for Allen-Cahn (top row)**: Distribution of RBA weights for Fitting (I), Transitional (II), and Diffusion (III) phases for the Allen-Cahn problem. The weights undergo a swift change from order to disorder at  $2 \cdot 10^4$  iterations, where they stop following the flow of information imposed by the initial condition. **Gradient distributions of network weights (middle row)**: Corresponding  $\|\mu\|$ ,  $\|\sigma\|$  and  $SNR$  curves for each layer, which indicate a high  $SNR$  during the fitting phase followed by a low  $SNR$  during the diffusion phase, as proposed by the IB theory. **Convergence history (bottom row)**: Convergence of normalized Loss/relative  $L^2$  and network weights  $\|w\|$ . Even though the Loss reaches a plateau after phase II, the relative  $L^2$  decreases quickly while the network weights begin their final convergence trajectory. Notably, the learning continues far beyond the convergence of the Loss.

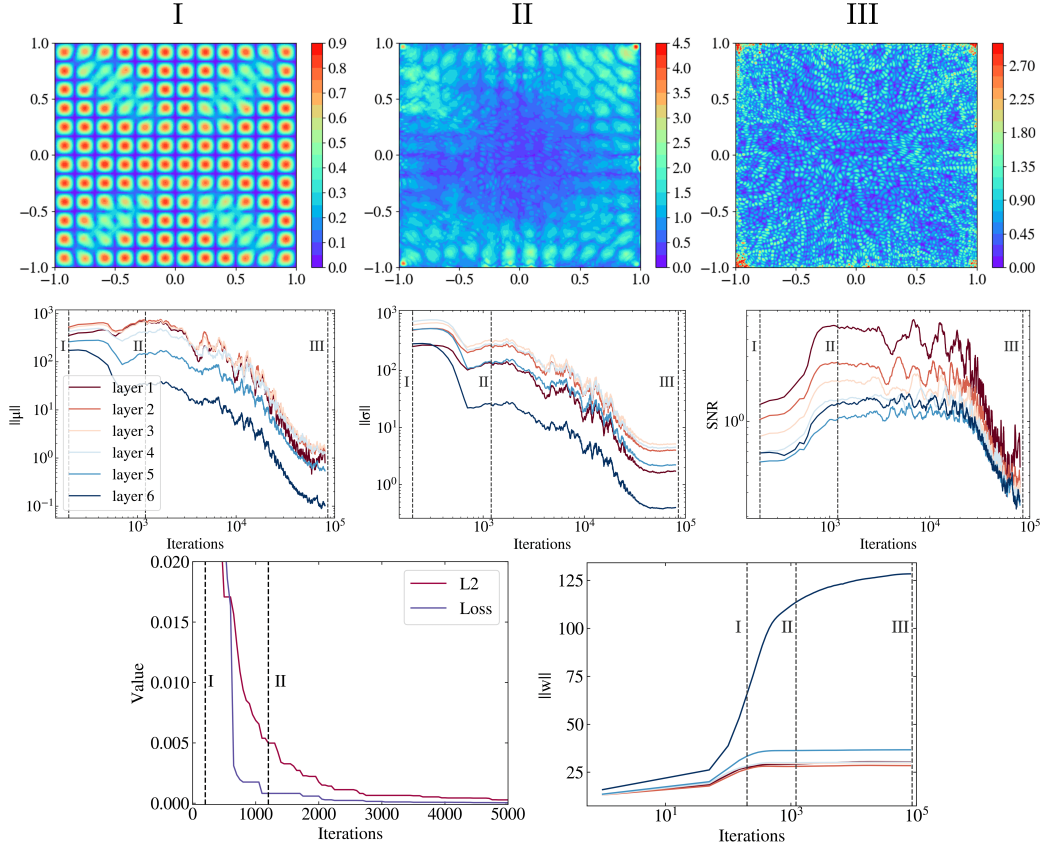


Figure 7: **Three phases of learning for Helmholtz (top row)**: Fitting (I), Transitional (II), and Diffusion (III) phases, during which the RBA weights distribution is presented. This case is run for  $10^5$  iterations to capture the final learning states fully. After 1400 iterations, the weights experience a rapid transition from an ordered to a disordered state, breaking away from the information flow dictated by the boundary conditions. **Gradient distributions of network weights (middle row)**: Gradient distributions of the network weights, displaying the corresponding  $\|\mu\|$ ,  $\|\sigma\|$  and  $SNR$  curves for each layer. This clearly indicates a high  $SNR$  in the fitting phase and a subsequent drop during the diffusion phase, aligning with the IB theory's predictions. **Convergence history (bottom row)**: Convergence of the normalized Loss/relative  $L^2$  and network weights  $\|w\|$ . Although the normalized Loss and relative  $L^2$  reach a plateau relatively early (after 5000 iterations), the Loss converges first around phase II. This is also concurrent with the final convergence trajectory onset of the network weights.

## 5. Summary

In this work, we propose a fast, residual-based attention scheme which can enhance the accuracy of PINNs in both static and dynamic cases, competing with the state-of-the-art performing models of the literature. Moreover, as the ablation study points out, a critical aspect of the solution accuracy is the formulation of exact boundary conditions. Additionally, even though the RBA multipliers provide considerable accuracy improvements, we believe that an equally important element of this type of weighting strategy is in the realms of convergence. For example, the 1D Allen-Cahn equation cannot be solved by the vanilla PINN due to its stiff nature, but RBA can initiate an early convergence trajectory. Furthermore, the versatility of the proposed method allows for its application with a few additional lines of code.

In addition, given that the adopted methodology can overcome a certain accuracy threshold, we provide evidence that the learning process is dominated by two distinct learning regimes, as suggested by the IB theory. In the first fitting phase, the model learns the most important parts of the solution. The distribution of the RBA weight values follows the main shape of the solution while it sets the stage for the next learning phase. In the diffusion phase, the weights stop following the flow of information from the initial conditions and start focusing on unregulated parts of the domain, resembling a diffusion process. Based on the IB theory, it is during this final phase that the model finds the best balance between detail and simplicity by tweaking what was learned in the fitting phase, hence refining its understanding of the problem.

This novel connection between IB theory and PINNs could open new possibilities for quantifying the performance of the many versions of PINNs and even neural operators. Furthermore, in applications where accuracy is essential, utilizing methods that collectively aid the optimizer in overcoming the threshold of the fitting phase could be a critical convergence criterion. Planned future work is focused on expanding the application of RBA weights to a broader spectrum of problems and testing the sensitivity of the associated hyperparameters. Additionally, we aim to undertake comprehensive parametric analyses of the bottleneck phase transition to enhance our understanding of its occurrence timing, underlying causes, and possible strategies to instigate it.

## Acknowledgements

SJA and NS thank the Swiss National Science Foundation grant “Hemodynamics of Physiological Aging” (Grant nr 205321\_197234). JDT and GEK acknowledge support by the DOE SEA-CROGS project (DE-SC0023191), the MURI-AFOSR FA9550-20-1-0358 project, and the ONR Vannevar Bush Faculty Fellowship (N00014-22-1-2795). Finally, we extend our gratitude to Prof. N. Sukumar from the University of California, Davis, for engaging in insightful discussions on the approximate distance functions.

## Appendix A. Implementation Details

The chosen architecture for all benchmarks is an MLP of 6 hidden layers and 128 neurons per layer, using the hyperbolic tangent (*tanh*) activation function. The weights are initialized with Xavier normal distribution [29]. The rest of the case-specific information and their corresponding training time is tabulated in the following sections. However, the reported training times should be used only as an inner reference since the codes were not optimized for speed.

### *Appendix A.1. Allen-Cahn*

Implementation Details	
Sampling method	Latin Hypercube
Number of collocation points	25600
Number of initial condition points	512
Initial learning rate	1e-3
Decay rate	0.9
Decay step	5000
ML framework	PyTorch
GPU	GeForce RTX 3090

Table A.6: Allen Cahn Implementation Details

Method	Training time (ms/iteration)
Vanilla	17
RBA	17
RBA+mMLP	58
RBA+Fourier	19
mMLP+Fourier	60
RBA+mMLP+Fourier	61

Table A.7: Comparison of computational speed for different combinations of the ablation study for the 1D Allen-Cahn equation.

*Appendix A.2. Helmholtz*

Implementation Details	
Sampling method	Uniform grid
Number of collocation points	1201
Number of boundary points (Fourier)	200
Initial learning rate	5e -3
Decay rate	0.7
Decay step	1000
ML framework	Jax
GPU	GeForce RTX 3090

Table A.8: Helmholtz ( $a_1 = 1, a_2 = 4$ ) Implementation Details

Method	Training time (ms/iteration)
Vanilla	13.8
RBA	13.8
RBA+mMLP	18.6
RBA+Fourier	22.6
mMLP+Fourier	37.8
RBA+mMLP+Fourier	34.4
RBA+ADF	14.2
mMLP+ADF	18.4
RBA+mMLP+ADF	18.6

Table A.9: Training time for 2D Helmholtz ( $a_1 = 1, a_2 = 4$ )

*Appendix A.3. 2D Helmholtz-Bottleneck*

Implementation Details	
Number of collocation points	90400
Initial learning rate	5e -3
Decay rate	0.7
Decay step	1000
ML framework	Jax
GPU	GeForce RTX 3090
Training time per iteration	88.4ms

Table A.10: Helmholtz ( $a_1 = 6, a_2 = 6$ ) Implementation Details

**Appendix B. Snapshots of weights and residuals**

This section displays indicative snapshots of the RBA weights and the corresponding residual evolution for the Allen-Cahn and Helmholtz models. As stipulated by the information bottleneck theory, during the training process we can observe the fitting, transition, and diffusion learning phases. The interplay between weights and residuals is evident as the former keep track of the short-term residual history. Therefore, the RBA weights may differ from the network’s residuals during the early iterations but as the latter stabilize in the final stages of convergence, the weights tend to follow suit, reflecting the trends observed in the PDE residuals.



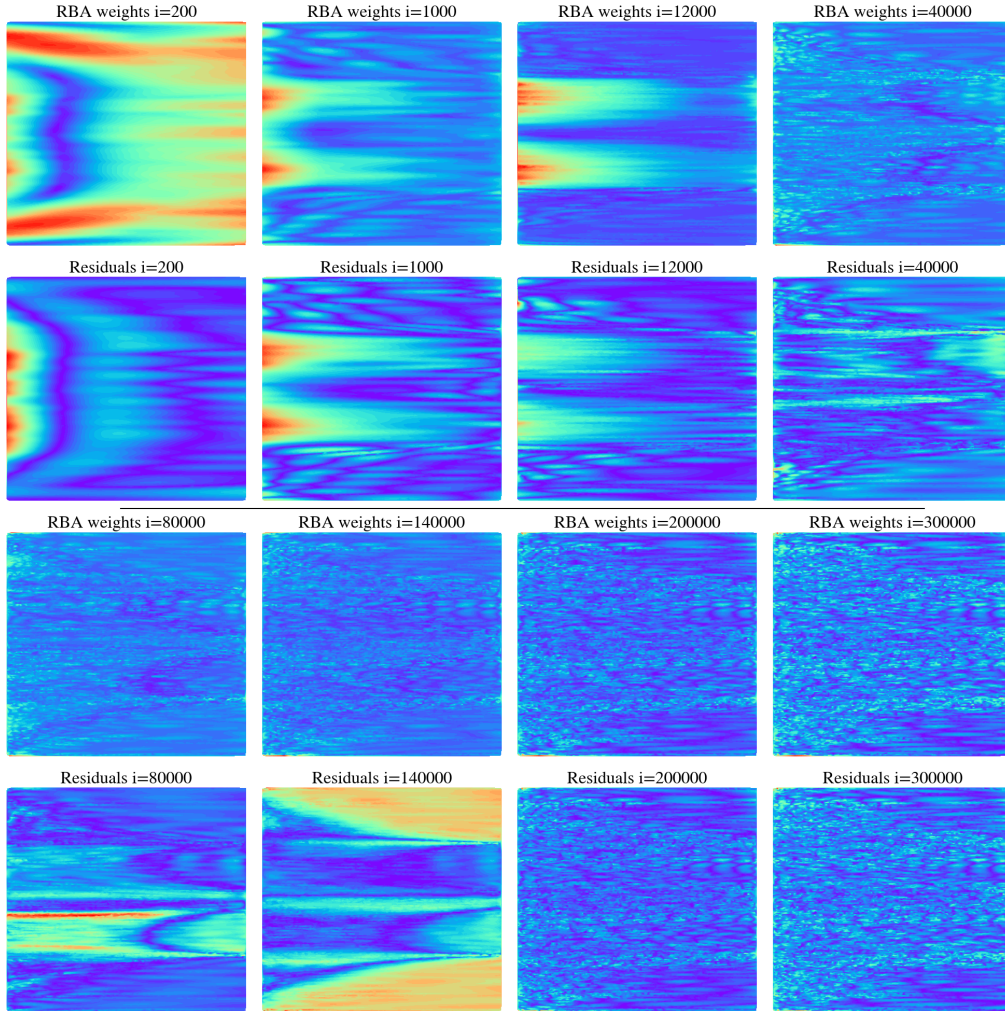


Figure B.8: **Snapshots of weights and residuals for the Allen-Cahn PDE.** We show results up to  $3 \cdot 10^5$  iterations to capture fitting, transition, and diffusion learning phases. The fitting phase ends around iteration 20000 while the weights experience a transition from order to disorder, breaking away from the information flow dictated by the initial condition. After the transition phase is over, the diffusion state is predominant around  $i=40000$ . During this chaotic phase, the SNR decreases and the model randomly focuses on refining scattered parts of the domain.

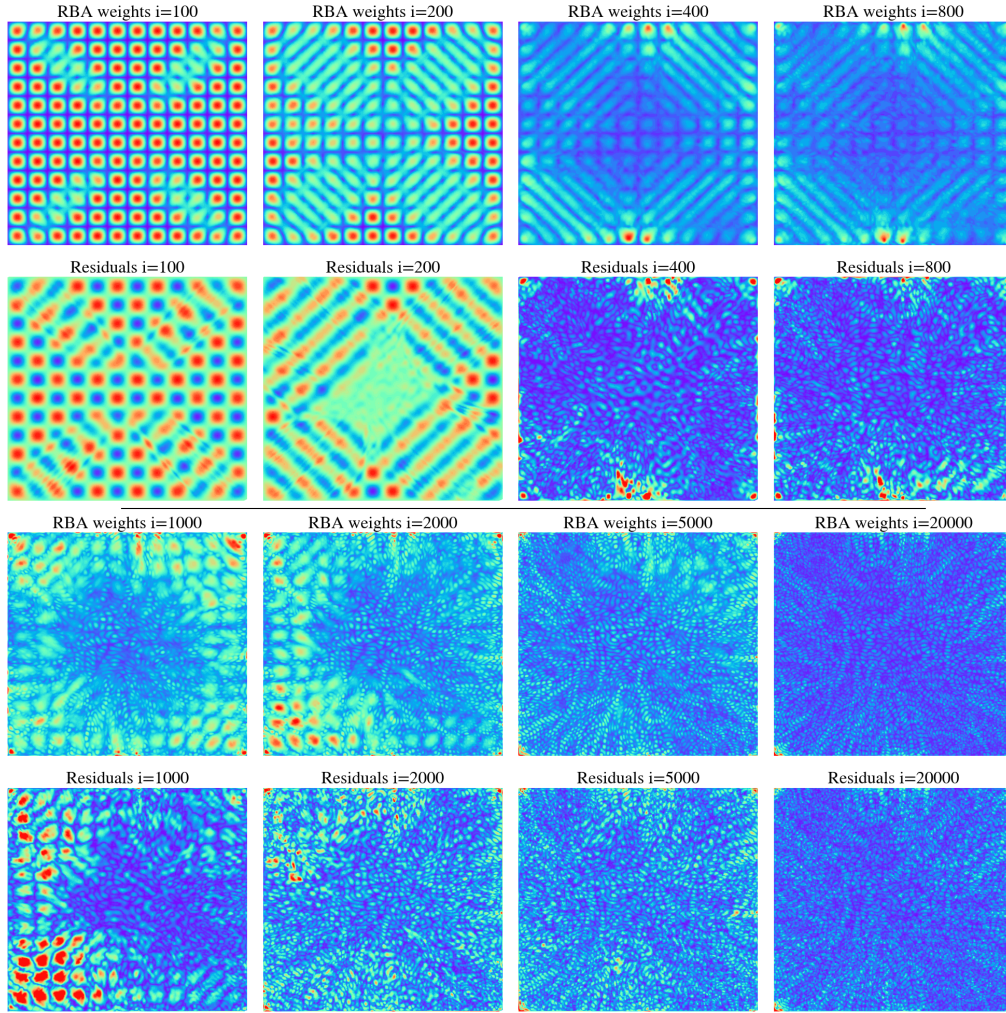


Figure B.9: **Snapshots of weights and residuals for Helmholtz** ( $a_1 = 6, a_2 = 6$ ). Results are shown for a total of  $2 \cdot 10^4$  iterations, capturing the fitting, transition, and diffusion learning phases. During the first 800 iterations, the fitting phase is dominant and the weights follow a specific order dictated by the trigonometric shape of the PDE solution. After that, the transition phase starts and the RBA weights rapidly switch to a disordered state. From 5000 iterations and onward, the system is primarily ruled by diffusion, causing the RBA weights to become chaotic and focus on optimizing unregulated regions of the domain.

## References

- [1] M. Raissi, P. Perdikaris, G. E. Karniadakis, Physics-informed neural networks: A deep learning framework for solving forward and inverse problems involving nonlinear partial differential equations, *Journal of Computational physics* 378 (2019) 686–707.
- [2] S. Cai, Z. Mao, Z. Wang, M. Yin, G. E. Karniadakis, Physics-informed neural networks (pinns) for fluid mechanics: A review, *Acta Mechanica Sinica* 37 (12) (2021) 1727–1738.
- [3] S. Wang, S. Sankaran, P. Perdikaris, Respecting causality is all you need for training physics-informed neural networks, *arXiv preprint arXiv:2203.07404* (2022).
- [4] L. McClenny, U. Braga-Neto, Self-adaptive physics-informed neural networks using a soft attention mechanism, *arXiv preprint arXiv:2009.04544* (2020).
- [5] V. A. Es'kin, D. V. Davydov, E. D. Egorova, A. O. Malkhanov, M. A. Akhukov, M. E. Smorkalov, About optimal loss function for training physics-informed neural networks under respecting causality, *arXiv preprint arXiv:2304.02282* (2023).
- [6] S. Wang, Y. Teng, P. Perdikaris, Understanding and mitigating gradient flow pathologies in physics-informed neural networks, *SIAM Journal on Scientific Computing* 43 (5) (2021) A3055–A3081.
- [7] T. Salimans, D. P. Kingma, Weight normalization: A simple reparameterization to accelerate training of deep neural networks, *Advances in neural information processing systems* 29 (2016).
- [8] W. Guan, K. Yang, Y. Chen, Z. Guan, A dimension-augmented physics-informed neural network (dapinn) with high level accuracy and efficiency, *arXiv preprint arXiv:2210.13212* (2022).
- [9] S. Wang, H. Wang, P. Perdikaris, On the eigenvector bias of fourier feature networks: From regression to solving multi-scale pdes with physics-informed neural networks, *Computer Methods in Applied Mechanics and Engineering* 384 (2021) 113938.

- [10] A. Krishnapriyan, A. Gholami, S. Zhe, R. Kirby, M. W. Mahoney, Characterizing possible failure modes in physics-informed neural networks, *Advances in Neural Information Processing Systems* 34 (2021) 26548–26560.
- [11] C. L. Wight, J. Zhao, Solving allen-cahn and cahn-hilliard equations using the adaptive physics informed neural networks, *arXiv preprint arXiv:2007.04542* (2020).
- [12] A. D. Jagtap, K. Kawaguchi, G. E. Karniadakis, Adaptive activation functions accelerate convergence in deep and physics-informed neural networks, *Journal of Computational Physics* 404 (2020) 109136.
- [13] N. Sukumar, A. Srivastava, Exact imposition of boundary conditions with distance functions in physics-informed deep neural networks, *Computer Methods in Applied Mechanics and Engineering* 389 (2022) 114333.
- [14] C. Leake, D. Mortari, Deep theory of functional connections: A new method for estimating the solutions of partial differential equations, *Machine learning and knowledge extraction* 2 (1) (2020) 37–55.
- [15] L. Lu, R. Pestourie, W. Yao, Z. Wang, F. Verdugo, S. G. Johnson, Physics-informed neural networks with hard constraints for inverse design, *SIAM Journal on Scientific Computing* 43 (6) (2021) B1105–B1132.
- [16] X. Jin, S. Cai, H. Li, G. E. Karniadakis, Nsfnets (navier-stokes flow nets): Physics-informed neural networks for the incompressible navier-stokes equations, *Journal of Computational Physics* 426 (2021) 109951.
- [17] S. Basir, Investigating and mitigating failure modes in physics-informed neural networks (pinns), *arXiv preprint arXiv:2209.09988* (2022).
- [18] L. Lu, X. Meng, Z. Mao, G. E. Karniadakis, Deepxde: A deep learning library for solving differential equations, *SIAM review* 63 (1) (2021) 208–228.
- [19] C. Wu, M. Zhu, Q. Tan, Y. Kartha, L. Lu, A comprehensive study of non-adaptive and residual-based adaptive sampling for physics-informed neural networks, *Computer Methods in Applied Mechanics and Engineering* 403 (2023) 115671.

- [20] B. Zapf, J. Haubner, M. Kuchta, G. Ringstad, P. K. Eide, K.-A. Mardal, Investigating molecular transport in the human brain from mri with physics-informed neural networks, *Scientific Reports* 12 (1) (2022) 15475.
- [21] Z. Xiang, W. Peng, X. Liu, W. Yao, Self-adaptive loss balanced physics-informed neural networks, *Neurocomputing* 496 (2022) 11–34.
- [22] D. Liu, Y. Wang, A dual-dimer method for training physics-constrained neural networks with minimax architecture, *Neural Networks* 136 (2021) 112–125.
- [23] G. Zhang, H. Yang, F. Zhu, Y. Chen, et al., Dasa-pinns: Differentiable adversarial self-adaptive pointwise weighting scheme for physics-informed neural networks, *SSRN* (2023).
- [24] N. Tishby, F. C. Pereira, W. Bialek, The information bottleneck method, *arXiv preprint physics/0004057* (2000).
- [25] N. Tishby, N. Zaslavsky, Deep learning and the information bottleneck principle, in: *2015 IEEE Information Theory Workshop (ITW)*, IEEE, 2015, pp. 1–5.
- [26] R. Shwartz-Ziv, N. Tishby, Opening the black box of deep neural networks via information, *arXiv preprint arXiv:1703.00810* (2017).
- [27] A. M. Saxe, Y. Bansal, J. Dapello, M. Advani, A. Kolchinsky, B. D. Tracey, D. D. Cox, On the information bottleneck theory of deep learning, *Journal of Statistical Mechanics: Theory and Experiment* 2019 (12) (2019) 124020.
- [28] Z. Goldfeld, Y. Polyanskiy, The information bottleneck problem and its applications in machine learning, *IEEE Journal on Selected Areas in Information Theory* 1 (1) (2020) 19–38.
- [29] X. Glorot, Y. Bengio, Understanding the difficulty of training deep feed-forward neural networks, in: *Proceedings of the thirteenth international conference on artificial intelligence and statistics, JMLR Workshop and Conference Proceedings*, 2010, pp. 249–256.

- [30] A. Vaswani, N. Shazeer, N. Parmar, J. Uszkoreit, L. Jones, A. N. Gomez, L. Kaiser, I. Polosukhin, Attention is all you need, *Advances in neural information processing systems* 30 (2017).
- [31] S. Dong, N. Ni, A method for representing periodic functions and enforcing exactly periodic boundary conditions with deep neural networks, *Journal of Computational Physics* 435 (2021) 110242.
- [32] J. Chen, R. Du, K. Wu, A comparison study of deep galerkin method and deep ritz method for elliptic problems with different boundary conditions, *arXiv preprint arXiv:2005.04554* (2020).
- [33] D. P. Kingma, J. Ba, Adam: A method for stochastic optimization, *arXiv preprint arXiv:1412.6980* (2014).
- [34] R. Matthey, S. Ghosh, A novel sequential method to train physics informed neural networks for allen cahn and cahn hilliard equations, *Computer Methods in Applied Mechanics and Engineering* 390 (2022) 114474.
- [35] J. D. Toscano, C. Zuniga-Navarrete, W. D. J. Siu, L. J. Segura, H. Sun, Teeth mold point cloud completion via data augmentation and hybrid rl-gan, *Journal of Computing and Information Science in Engineering* 23 (4) (2023) 041008.